Dynamic DH-MBIR for low-latency wavefront estimation in the presence of atmospheric boiling

Ali G. Sheikh[a], Casey J. Pellizzari[b], Sherman J. Kisner[c],
Gregery T. Buzzard[d], and Charles A. Bouman[e]

[a,d,e]Purdue University, West Lafayette, IN, USA
[b]United States Air Force Academy, Colorado Springs, CO, USA
[c]High Performance Imaging LLC, West Lafayette, IN, USA

ABSTRACT

The estimation of phase errors due to atmospheric turbulence from digital-holography (HD) data with high throughput and low latency is critical for applications such as wavefront sensing and directed energy. The problem of focusing outgoing directed energy is particularly difficult because the phase errors must be estimated with extremely low latency for use in closed-loop correction of the outgoing light before the atmospheric parameters decorrelate. This low latency requirement necessitates that the phase distortion be estimated from a single shot of DH data. The Dynamic DH-MBIR (DDH-MBIR) algorithm has been shown to be capable of accurately estimating isoplanatic phase-errors using the expectation-maximization (EM) algorithm; however, DDH-MBIR was introduced using data that models only frozen flow of atmospheric turbulence.

In this paper, we characterize the performance of the Dynamic DH-MBIR algorithm in more realistic settings. Specifically, Dynamic DH-MBIR produces accurate phase estimates in the case of moderate levels of atmospheric boiling.

Keywords: Coherent Imaging, Phase Retrieval, Atmospheric Turbulence, Digital Holography, Directed Energy, Wavefront Sensing

1. INTRODUCTION

The goal of a directed energy system is to focus a beam of light on a distant object. In terrestrial applications, this can be difficult because atmospheric turbulence introduces random phase errors (or distortions) that tend to disperse the otherwise focused beam. A solution to this problem is to pre-distort the phase of the outgoing beam. This can be done by first performing wavefront sensing (WFS), in which the phase distortion of incoming light is measured. The outgoing light can then be pre-distorted with the conjugate phase. However, this approach requires that the WFS be performed with very low latency, so that the phase corrections can be applied before the atmospheric distortion changes.

Digital holography (DH) sensors can be used to estimate the wavefront from direct measurements of the light. DH sensors measure the amplitude and phase of incoming light by interfering the received light with a reference beam. The resulting complex-valued measurements can then be used to computationally estimate phase distortions by solving an inverse problem.[1] We previously introduced[2] the Dynamic DH-MBIR algorithm (DDH-MBIR) that can accurately estimate phase-errors due to atmospheric turbulence while meeting the low-latency and high-throughput requirements of applications such as directed energy.

In this paper, using simulations, we characterize the performance of DDH-MBIR under a more realistic atmospheric turbulence model that includes boiling effects. DDH-MBIR achieves an average Strehl ratio over roughly 0.8 for a boiling level of 10% and an average Strehl ratio above 0.5 of a boiling level of 15%.

Further author information: (Send correspondence to A.G.S.)
A.G.S.: E-mail: sheikh4@purdue.edu
C.J.P.: E-mail: casey.pellizzari@afacademy.af.edu
S.J.K: Email: sherman.kisner@highperformanceimaging.com
G.T.B: Email: buzzard@purdue.edu
C.A.B: Email: bouman@purdue.edu

2. DYNAMIC DH-MBIR

2.1 Forward Model

A DH sensor allows us to measure the complex electromagnetic field reflected from an object using spatial-heterodyne interferometry. As in Pellizzari, et al.,[3] we model the complex-valued measurements at time n as

$$y_n = A_{\phi_n} g_n + w_n, \tag{1}$$

where $y_n \in \mathbb{C}^M$ is the rasterized vector of complex DH measurements, $g_n \in \mathbb{C}^M$ is the vector of unknown complex reflection coefficients from the illuminated object, $w_n \in \mathbb{C}^M$ is a vector of complex measurement noise, and $A_{\phi_n} \in \mathbb{C}^{M \times M}$ is a linear transformation that is dependent on the unknown phase error, ϕ_n.

If the wavelength of the light is small compared to the resolved pixel size on the object, then the reflection coefficient, g_n, is accurately modeled as a circularly symmetric, complex Gaussian with unknown variance, r_n. In this case, r_n is real-valued reflectance with $r_n = E[|g_n|^2]$ and $g_n \sim CN(0, r_n)$.

We assume an isoplanatic propagation model in which the phase distortion, ϕ_n, occurs close to the detector.[4] The isoplanatic linear forward model can be decomposed as

$$A_{\phi_n} = D_a \mathcal{D}(e^{j\phi_n}) F \Gamma$$

where D_a is a diagonal matrix that models the camera aperture, $\mathcal{D}(e^{j\phi_n})$ is a diagonal matrix of phase distortions, F is a normalized 2D discrete Fourier transform (DFT), and Γ is a diagonal matrix of quadratic phase factors resulting from Fresnel propagation.[5]

2.2 Dynamic DH-MBIR Algorithm

The Dynamic DH-MBIR (DDH-MBIR) algorithm estimates r_n and ϕ_n from a streaming sequence of DH data, y_n. As previously specified,[2] DDH-MBIR uses the expectation-maximization (EM) algorithm to solve the joint-MAP estimate

$$(\hat{r}_n, \hat{\phi}_n) = \arg\min_{r,\phi} \{ -\log p(y_n | r, \phi) - \log p(r) - \log p(\phi) \}. \tag{2}$$

The key innovation of the DDH-MBIR algorithm is the initialization of r_n given by

$$r_n^{init} \leftarrow (1-\lambda) \underbrace{r_{n-1}}_{1^{st} \text{ term}} + \lambda\alpha \underbrace{|A_{\phi_{n-1}}^H y_n|^2}_{2^{nd} \text{ term}} . \tag{3}$$

This initialization leverages the temporal correlation of both ϕ and r. It is formed by a weighted sum of two terms where λ and α are user selectable weights in the range $[0, 1]$. Since r does not typically change substantially between samples, the first term, r_{n-1}, provides a good initial condition for the estimation of r_n.

The second term uses the magnitude squared of the back-projected data. Intuitively, this second term incorporates a small amount of continuous bootstrapping into the dynamic update loop, which keeps the DDH-MBIR output away from solutions associated with local minima.

In this paper, we fix the number of iterations/timestep to 1. Figure 1 shows the pseudo-code and a flow diagram for DDH-MBIR. The computation of the $EM()$ function is dominated by the application of two FFTs.[6] The RemoveTipTilt() function removes the linear component of the phase corresponding to spatial shifts of the reconstructed image.

3. EXPERIMENTAL RESULTS

In this section, we present estimation results from synthetic data using the Dynamic DH-MBIR algorithm.

function DDH_MBIR(λ, α, N_k)
  $n \leftarrow 0$; $r \leftarrow 0$; $\phi \leftarrow 0$
  while Data is available **do**
    $y \leftarrow \text{ReadData}(n)$
    $y \leftarrow \text{Normalize}(y)$
    $\phi \leftarrow \text{RemoveTipTilt}(\phi)$
    $r \leftarrow (1-\lambda)r + \frac{1}{2}\lambda\alpha \left|A_\phi^H y\right|^2$
    $(r, \phi) \leftarrow EM(r, \phi; y)$
    $\text{WriteData}(n, r, \phi)$
    $n \leftarrow n + 1$
  end while
end function

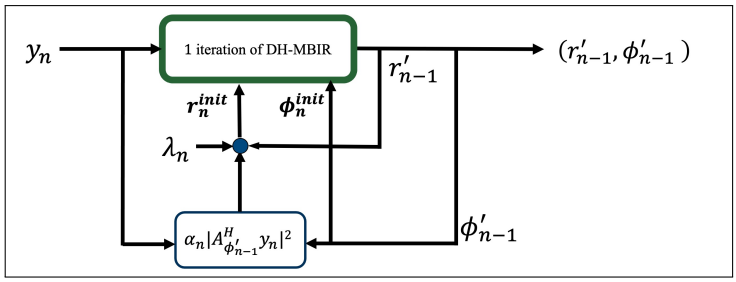

Figure 1: Left: Pseudo-code for the Dynamic DH-MBIR algorithm. Each iteration initializes r with a weighted combination of the previous estimate and a back-projection of the DH data. Right: DDH-MBIR flow diagram.

3.1 Atmospheric Turbulence Model

Phase-errors due to atmospheric turbulence, at any given time n, are modeled as a single phase screen placed near the detector; this is called the isoplanatic case. Wind and atmospheric boiling are the two dominant forces of change of the phase screen as a function of time n. Wind is modeled as a spatial shift in the phase screen in a particular direction and with a certain speed. Atmospheric boiling is modeled as the addition of a phase screen with certain properties that are stochastic in nature. To run simulations in a computationally feasible manner, we use the auto-regressive method developed in Srinath, et al.,[7] with modified von Karman statistics. The fraction of atmospheric boiling is specified by $b > 0$ in

$$\Phi_n = \tau\Phi_{n-1} + bP\Omega_n$$

where Φ_n is the Fourier transform of ϕ_n, τ is the complex-valued AR coefficient that also encodes the wind velocity, $b = \sqrt{1-|\tau|^2}$, P is the von Karman power spectral density, and Ω_n is the Fourier transform of white noise.

3.2 Data Simulation

We generated data using the 1951 USAF resolution test chart for r along with a phase-error model described above. At each timestep, the DH data, y_n, was generated as in Pellizzari, et al.[3] We also removed the piston, tip, and tilt of the phase-errors because we are interested only in estimating the higher-order aberrations.

Furthermore, we used an isoplanatic model, image and phase distortion array sizes of $N \times N$ where $N = 256$, a sampling frequency of $f_s = 10kHz$, a Greenwood frequency $f_g = 100Hz$, a turbulence strength of $D/r_0 = 10$ where D is the diameter of the aperture and r_0 is Fried's parameter,[8] a wavelength of $1.064\mu m$, and an SNR of $10dB$. Using these parameters, we find the magnitude of the phase displacement between time samples by scaling Equation 4.15 in Tyson[9] to convert from m/s to pixels/sample. This gives

$$\|v\| = \frac{1}{0.43}\frac{f_g}{f_s}\frac{N}{D/r_0} \ .$$

In our simulation we assumed a flow downward and to the right, which gives a vector displacement of $v = (0.421, 0.421)$ pixels per time step.

We set $\sigma_r = 2$ and $\sigma_\phi = 0.175$ for the potential functions in the prior models specified in Pellizzari, et al.[10]

3.3 Algorithm Parameters and Metrics

In all our simulations, the DDH-MBIR parameters are $\alpha = 0.0025$ and $\lambda = 0.25$. We found that these parameters worked best for each boiling level.

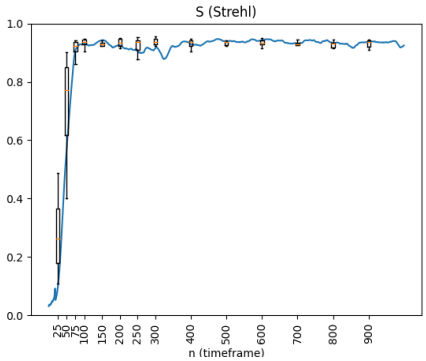

(a) $b = 0.03$

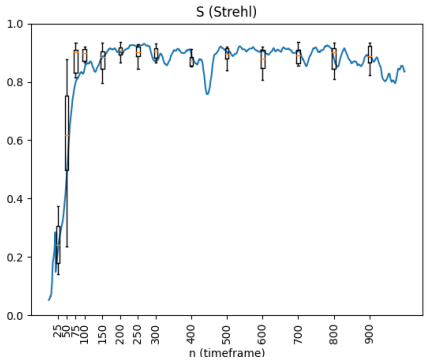

(b) $b = 0.06$

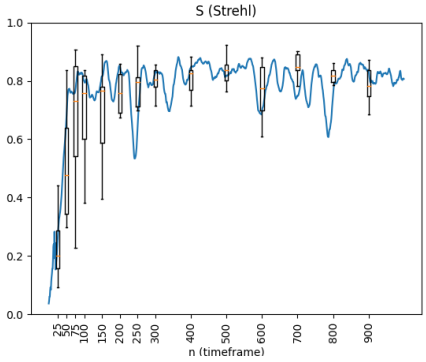

(c) $b = 0.1$

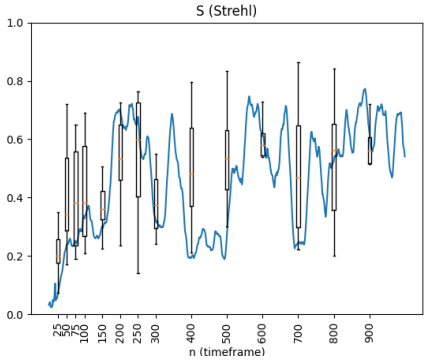

(d) $b = 0.15$

Figure 2: Box plots of Strehl ratio for 10 simulations of DDH-MBIR with the window-averaged (window size: 20 timesteps) Strehl curve of a particular simulation overlaid in blue. Each figure for a different boiling fraction, b. DDH-MBIR achieves a very good Strehl ratio through $b = 0.1$ and produces reasonable results even at $b = 0.15$.

We used peak Strehl ratio, S, to evaluate the quality of the phase-errors estimates, where

$$S = \frac{[|A^H_{\hat{\phi}_n - \phi_n} D_a|^2]_{\max}}{[|A^H_0 D_a|^2]_{\max}} \ ,$$

and $\hat{\phi}_n$ is the estimated phase, A^H_0 is back-propagation through a vacuum, and $[\cdot]_{\max}$ indicates the maximum value of the argument.

3.4 Results and Observations

Figure 2 shows box and whiskers plots of Strehl ratio as a function of time, averaged over 10 simulations, with results from a typical simulation overlaid in blue. Each plot is at a different boiling level. Figures 3, 4 and 5 show the true and estimated phase-errors at times $n = 0, 30,$ and 90 at boiling levels $b = 0.06$, 0.1, and 0.15, respectively. In figure 4, the estimate at $n = 90$ is quite close to the ground truth. This gives an additional viewpoint besides the Strehl ratio. At boiling level of $b = 0.15$, the phase estimate, shown in figure 5, shows a number of features of the ground truth at time $n = 90$.

From the top row in figure 5 we see how quickly the phase errors change from time $n = 30$ to $n = 90$ at this boiling level. For additional context, given the 10 kHz sampling rate, at boiling levels of $b > 0.1$ the phase errors look drastically different in less than 0.006 seconds.

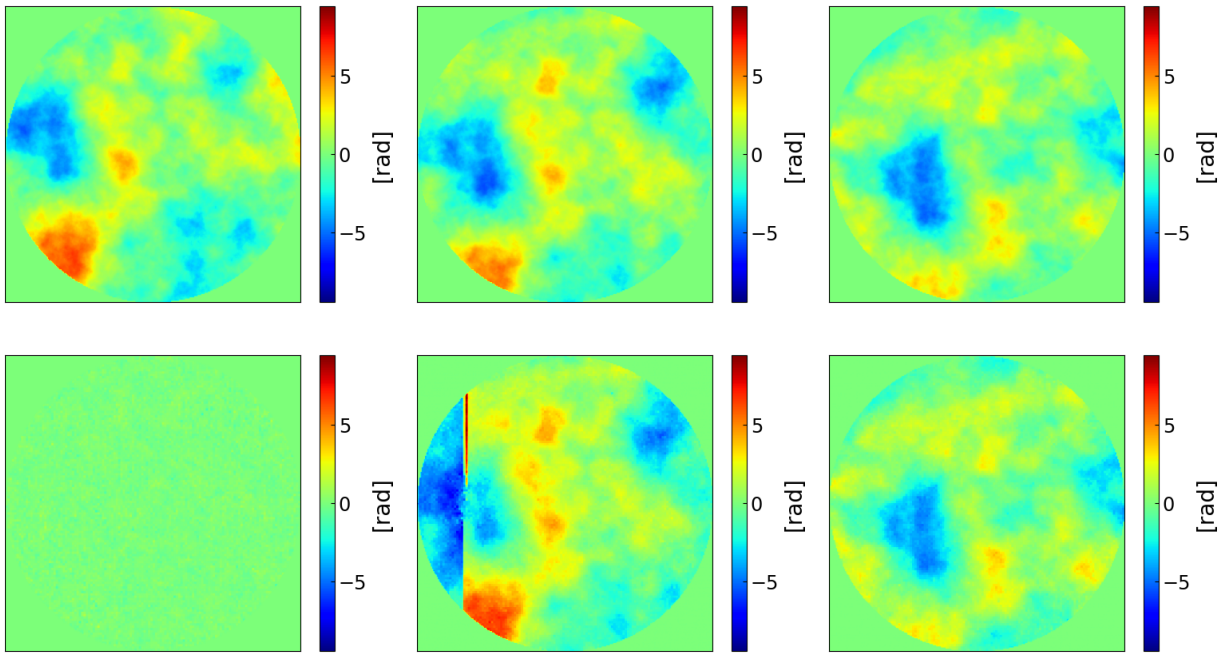

Figure 3: Boiling fraction $b = 0.06$. Top row: true phase-errors at times $n = 0, 30$, and 90 (from left to right). Bottom row: estimated phase-errors at times $n = 0, 30$, and 90 (from left to right). At low boiling levels, DDH-MBIR estimates the phase errors quickly and accurately.

Steady state Strehl, defined to be the average Strehl over timeframes $n = 500$ to $n = 1000$, gives us a single number to characterize the performance of DDH-MBIR. Figure 6 shows how the steady state Strehl changes with increased boiling.

4. CONCLUSION

We characterized the Dynamic DH-MBIR algorithm's performance, at the low latency requirement of only 1 iteration per timestep, under a realistic atmospheric turbulence model that includes wind and boiling. Dynamic DH-MBIR performs well with atmospheric boiling up to $b = 0.1$ when considering peak Strehl ratio and degrades gracefully through $b = 0.15$. However, we speculate that this could likely be even higher if we consider other metrics such as Power in the Bucket (PIB). And, in practice, the algorithm's peak Strehl at the boiling levels of $b = 0.15$ or higher may be adequate for practical application.

ACKNOWLEDGMENTS

This research was supported by the United States Air Force and the Air Force Research Laboratory. GTB was partially supported by NSF CCF-1763896. CAB was partially supported by the Showalter Trust. Approved for public release: distribution unlimited. The views expressed in this article, book, or presentation are those of the author and do not necessarily reflect the official policy or position of the United States Air Force Academy, the Air Force, the Department of Defense, or the U.S. Government.

REFERENCES

[1] Spencer, M. F., Raynor, R. A., Banet, M. T., and Marker, D. K., "Deep-turbulence wavefront sensing using digital-holographic detection in the off-axis image plane recording geometry," *Optical Engineering* **56**(3), 031213 (2016).

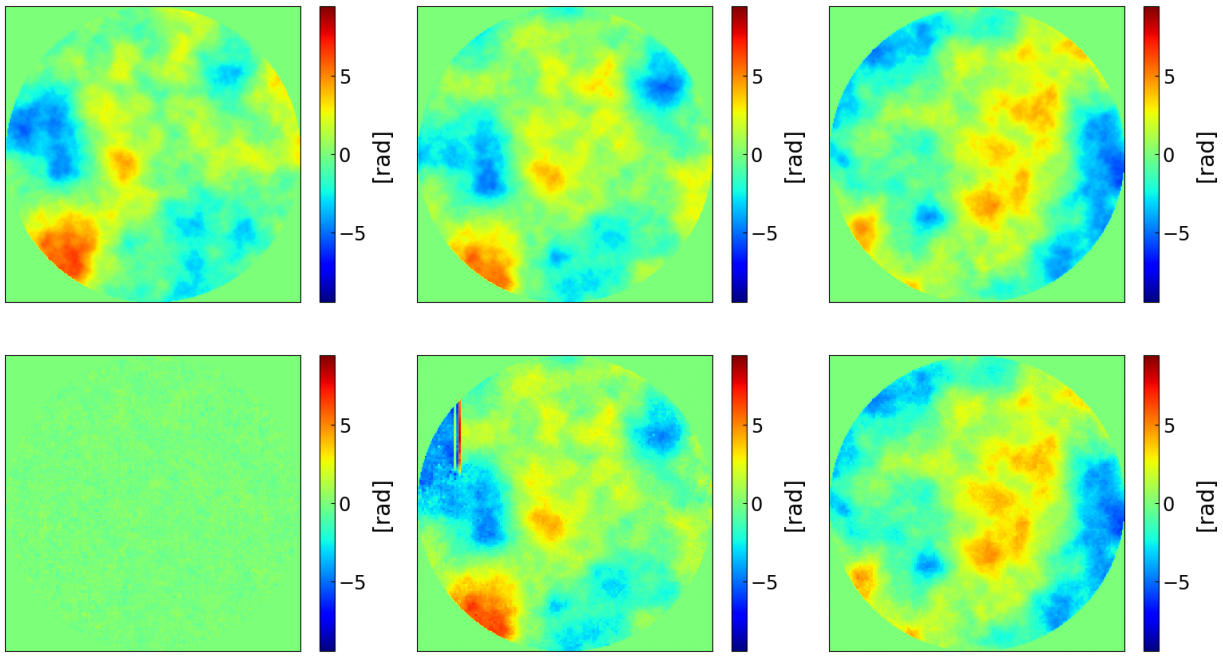

Figure 4: Boiling fraction $b = 0.1$. Top row: true phase-errors at times $n = 0, 30$, and 90 (from left to right). Bottom row: estimated phase-errors at times $n = 0, 30$, and 90 (from left to right). At this boiling level, DDH-MBIR takes a bit longer than at smaller boiling levels to capture the phase errors accurately but still achieves a consistently high Strehl ratio.

[2] Sheikh, A. G., Pellizzari, C. J., Kisner, S. J., Buzzard, G. T., and Bouman, C. A., "Dynamic DH-MBIR for phase-error estimation from streaming digital-holography data," (2023). Submitted to IEEE Asilomar, 2023.

[3] Pellizzari, C. J., Trahan, R., Zhou, H., Williams, S., Williams, S. E., Nemati, B., Shao, M., and Bouman, C. A., "Optically coherent image formation and denoising using a plug and play inversion framework," *Appl. Opt.* **56**, 4735–4744 (Jun 2017).

[4] Pellizzari, C. J., Spencer, M. F., and Bouman, C. A., "Imaging through distributed-volume aberrations using single-shot digital holography," *JOSA A* **36**(2), A20–A33 (2019).

[5] Schmidt, J. D., "Numerical simulation of optical wave propagation with examples in matlab," in [*Numerical simulation of optical wave propagation with examples in MATLAB*], SPIE Bellingham, WA (2010).

[6] Sridhar, V., Kisner, S. J., Midkiff, S. P., and Bouman, C. A., "Fast algorithms for model-based imaging through turbulence," in [*Artificial Intelligence and Machine Learning in Defense Applications II*], **11543**, 118360D, International Society for Optics and Photonics (SPIE) (2020).

[7] Srinath, S., Poyneer, L. A., Rudy, A. R., and Ammons, S. M., "Computationally efficient autoregressive method for generating phase screens with frozen flow and turbulence in optical simulations," *Opt. Express* **23**, 33335–33349 (Dec 2015).

[8] Fried, D. L., "Greenwood frequency measurements," *Journal of The Optical Society of America A-optics Image Science and Vision* **7**, 946–947 (1990).

[9] Tyson, R. K., [*Introduction to Adaptive Optics*], SPIE (Mar. 2000).

[10] Pellizzari, C. J., Spencer, M. F., and Bouman, C. A., "Phase-error estimation and image reconstruction from digital-holography data using a bayesian framework," *JOSA A* **34**(9), 1659–1669 (2017).

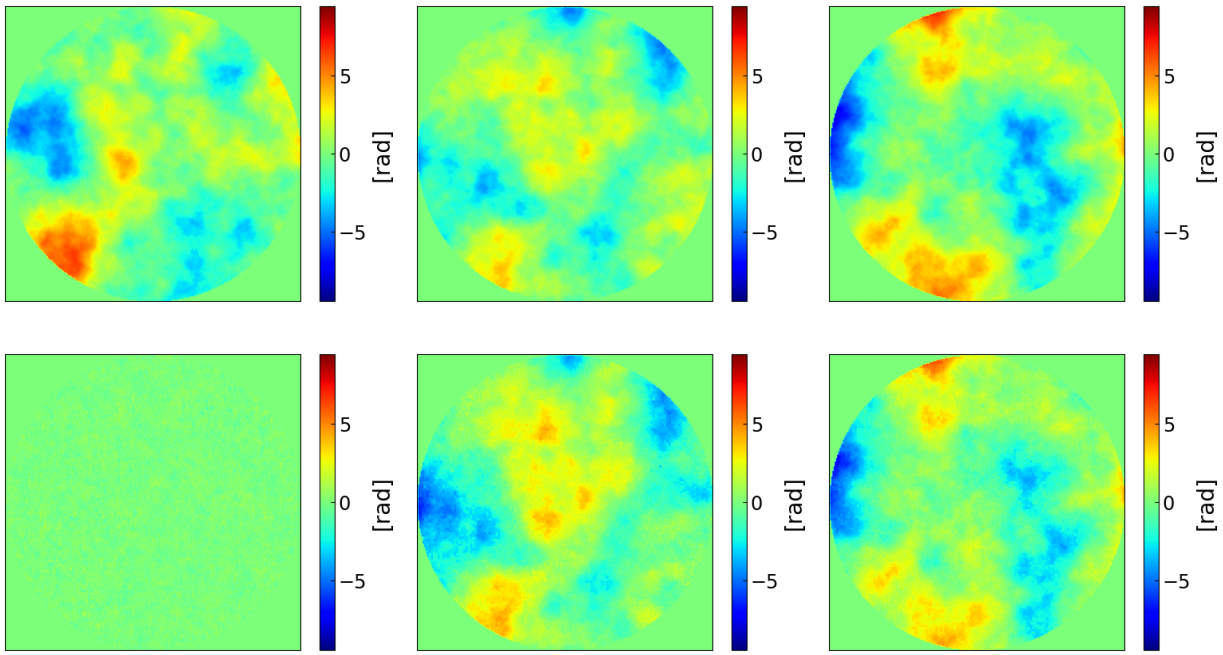

Figure 5: Boiling fraction $b = 0.15$. Top row: true phase-errors at times $n = 0, 30$, and 90 (from left to right). Bottom row: estimated phase-errors at times $n = 0, 30$, and 90 (from left to right). At this boiling level, DDH-MBIR is able to track the large scale features of the phase errors but is not completely accurate at fine scales.

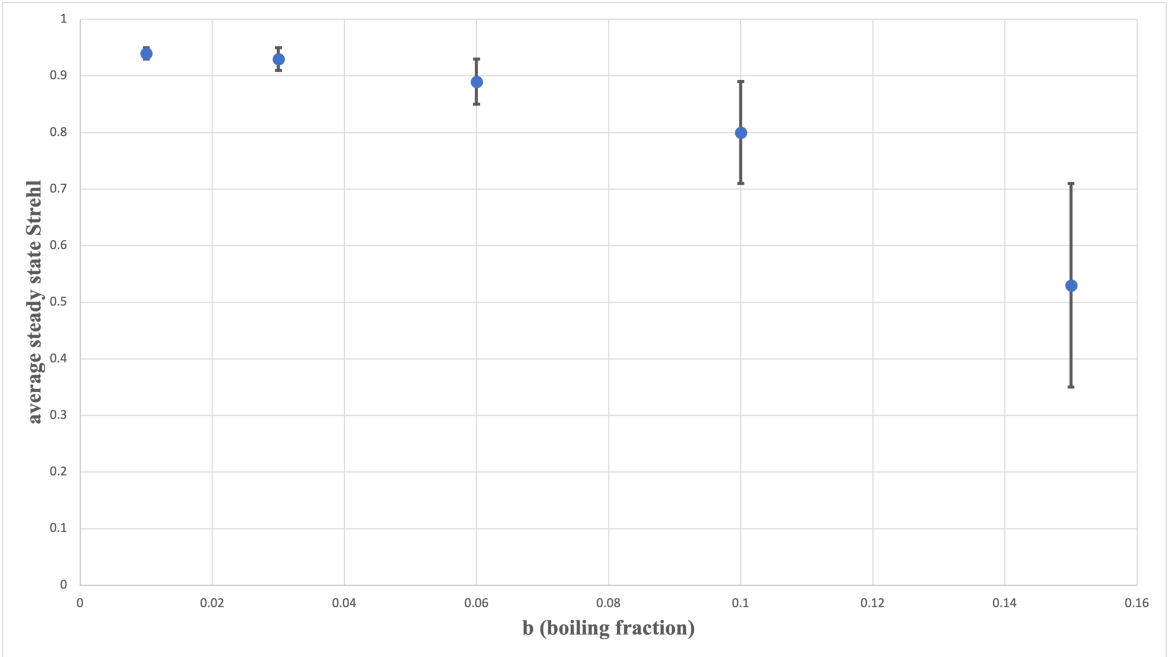

Figure 6: Steady state Strehl ratio averaged over 10 simulations as a function of boiling fraction. Steady state Strehl is defined as the average Strehl over timeframes $n = 500$ to $n = 1000$. The average Strehl ratio stays above 0.8 through a boiling fraction of 10% and degrades gracefully for boiling fractions through 15%.